Surface and near-surface modifications and analysis by MeV ions

B. N. Dev

Institute of Physics, Sachivalaya Marg, Bhubaneswar 751 005, India

Ion accelerators providing ions up to a few MeV energies have become an important research tool in materials and surface science. In industry, such accelerators are used for fabrication as well as analysis. With the installation of a 3 MV Pelletron accelerator in our Ion Beam Laboratory, ion beam analytical techniques were set up in 1991 and an ion implantation facility, somewhat later. The essence of the research programme dealing with surface phenomena, diffusion, epitaxial layer growth on surfaces, analysis of strain and defects, surface modifications by ion beams and exploration of coherent dynamic effect in the response of electrons in the interaction of cluster-ions with solids is presented here.

1. Introduction

THE knowledge of basic ion–solid interaction phenomena has contributed greatly to materials science. The research area of materials modification and analysis using energetic ion beams from accelerators has developed over the past three decades. Several international conferences are being held every year[1]. In surface and interface science, the analytical techniques using accelerated ion beams are used in addressing both fundamental and technological issues.

Much of our understanding of solids is based on the fact that they are, in essence, perfectly periodic in three dimensions. The introduction of a surface breaks this periodicity in one direction. This can lead to structural changes on the surface and consequently many properties of the surface differ from those of the bulk solid.

Ion beam analysis (IBA) has been used to study surface relaxation and reconstruction, i.e., the structural changes upon creation of the surface[2,3]. Growth of epitaxial (crystalline) layers on single crystalline solid surfaces, strain in the epilayer, defects in the epilayer and at the buried layer/substrate interface, diffusion across interfaces, crystal growth in solid phase epitaxy and other aspects relating to surface, interface and thin films are routinely studied using the IBA techniques.

e-mail: bhupen@iopb.res.in

Ion beam modification (IBM) is used to modify a near-surface region of materials by exposing them to various energetic ions and often incorporating the ions into them. Thus increase of surface hardness, fabrication of *n*- or *p*-type electrically active layers or insulating layers, creation of a buried epitaxial layer with Schottky barriers at the interfaces, creation of embedded quantum dots with nonlinear optical behaviour are some of the areas where IBM has contributed. Most of the earlier studies and technological uses involved monatomic ions. In recent years there has been an interest in the study of interactions of cluster-ions with solids.

In this article, some of the aspects mentioned above regarding surface, interface and thin films will be discussed with examples taken from the work done in our laboratory. These studies involve X-ray characterizations and use of various ions of a few MeV energy for both IBA and IBM experiments. Surface and interface characterizations with high resolution X-ray diffraction, X-ray reflectometry and X-ray standing waves have been presented elsewhere[4]. Here we restrict our discussions to ion beam analysis and ion beam modifications. For IBA we perform mainly Rutherford backscattering spectrometry and ion channeling experiments. These techniques and the experimental set-up in our Ion Beam Laboratory with the 3 MV Pelletron accelerator have been described earlier by Sekar *et al.*[5,6]. The principles of RBS and channeling are briefly discussed in the following section.

2. Rutherford backscattering spectrometry and channeling

2.1 *Rutherford backscattering spectrometry*

In this section we briefly describe various aspects of Rutherford backscattering spectrometry (RBS), the ion channeling phenomenon and RBS under channeling condition. More details may be obtained in refs 2 and 5.

In RBS, one is concerned with incident ions of a given energy that move through a sample, losing energy along their path, and are scattered by collision with atoms in the sample. The ions scattered in the backward

direction are detected and energy-analysed to obtain information about various aspects of the sample. The interaction between a projectile (ion) and a target (sample) atom can be described as an elastic collision between two isolated particles and expressed in terms of a *scattering cross section*. The energy of the projectile after the collision can be related to its energy before the collision by means of a *kinematic factor*. As the ion passes through the scattering medium, it suffers an average energy loss dE/dx. Thus the energy of a scattered ion not only depends upon the *kinematic factor* but also on the depth from the sample surface where the scattering occurs. The incident ion loses some energy to reach this depth and after scattering, it again loses some energy to come out of the sample from this depth. So the energy of the detected scattered ion contains the depth information.

2.1.1 Kinematic factor and the energy spectrum. When a particle of mass M_1 moving with a constant velocity collides elastically with a stationary particle of mass M_2, energy is transferred from the moving to the stationary particle. In backscattering analysis, mass M_1 is the mass of an ion in the analysing beam and M_2 is that of an atom in the sample. The energy E of the projectile after collision with the target atom, is related to its energy E_0 before the collision by the *kinematic factor K* defined by

$$E = KE_0, \tag{1}$$

where

$$K = \left[\frac{M_1\cos\theta + (M_2^2 - M_1^2\sin^2\theta)^{1/2}}{M_1 + M_2}\right]^2. \tag{2}$$

If ions of known mass M_1 and known energy E_0 are directed at a sample containing an element of unknown mass M_2, by measuring the energy (E) of ions scattered at an angle θ, the unknown mass M_2 can be determined.

2.1.2 Scattering cross section $d\sigma/d\Omega(\theta)$ *and the scattering yield.* In RBS, ions that are scattered by an angle θ are usually detected by a solid state detector that subtends a small solid angle Ω (typically less than 10^{-2} Sr). The yield or the number of counts, Y, registered by a 100% efficient detector is given by

$$Y = QNt\frac{d\sigma}{d\Omega}(\theta)\Omega, \tag{3}$$

where Q is the number of ions incident on the sample, N the bulk density of atoms in the sample, t the sample thickness and $d\sigma/d\Omega(\theta)$ the average differential scattering cross section for scattering into a solid angle Ω at a scattering angle θ. The differential cross section is given by Rutherford's formula (in laboratory frame of reference):

$$\frac{d\sigma}{d\Omega}(\theta) = \left[\frac{Z_1Z_2e^2}{4E}\right]^2 \frac{4}{\sin^4\theta} \tag{4}$$

$$\frac{\{[1-((M_1/M_2)\sin\theta)^2]^{1/2} + \cos\theta\}^2}{\{1-((M_1/M_2)\sin\theta)^2)^{1/2}},$$

where E is the energy of the ion immediately before scattering and Z_1 and Z_2 are the atomic numbers of the ion and the target atom respectively.

2.1.3 Energy loss of ions (dE/dx). As an energetic ion passes through a solid, it loses energy on its way. For light ions and for ion energies used in RBS analysis (0.1–3 MeV) there are two dominant energy loss processes: (i) By interactions with bound or free electrons in the solid [electronic energy loss: $(dE/dx)_e$] and (ii) by interactions with the screened or unscreened nuclei of the atoms in the solid [nuclear energy loss: $(dE/dx)_n$]. From the knowledge of the total $dE/dx = (dE/dx)_n + (dE/dx)_e$ for a given ion in a given sample material, the thickness (Δx) of thin film samples can be determined from the measured energy width (ΔE) in the RBS spectrum. This is illustrated in Figure 1 which shows schematically an RBS spectrum from a sample containing a thin film of a compound (two elements) on a thick substrate (single element).

When atoms from the top layer diffuse into the substrate, their existence at larger depths produces a tail on the low energy edge of the spectrum of the corresponding element. Diffusion coefficient can be determined from the analysis of this tail in the RBS spectra. This is

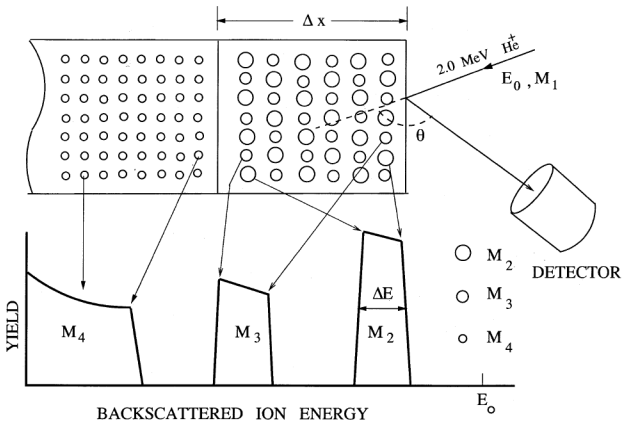

Figure 1. Schematic diagram of illustrating backscattering spectrum of ions of mass M_1 impinging on a thin film containing two different masses (M_2, M_3) deposited on a low-mass (M_4) elemental substrate. Energies of backscattered ions from various depths and various atoms are marked by arrows. The film thickness (Δx) is determined from the measured energy width ΔE.

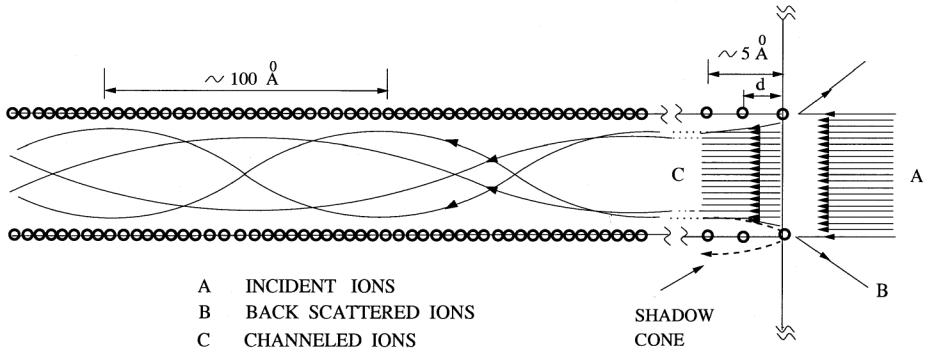

Figure 2. Schematic diagram showing trajectories of particles undergoing scattering at the surface and channeling within the crystal. The *shadow cone* behind the surface atoms is shown by dashed lines.

described in §3. Formation of nonuniform structures also gives rise to a broad tail in the backscattering spectrum. This is described in §4 in connection with the self-organized growth process on surfaces.

2.2 *Channeling*

When the incident direction of an ion beam is aligned with a crystallographic axis or plane of a single crystal sample, the majority of the ions penetrate (channel) into the crystal. Channeled particles cannot undergo large angle Rutherford scattering and hence the backscattering is drastically reduced – typically by a factor of about 50. The channeling phenomenon is described in Figure 2. The channeling effect occurs over a small angular range of the incident ion beam, expressed in terms of a *critical angle* (or half-angle) $\psi_{1/2}$. The value of $\psi_{1/2}$ depends on the type of ion, the ion energy, the type of sample crystal, specific crystallographic axis or plane along which the ion beam is incident and the thermal vibrational amplitude of constituent atoms in the sample crystal $\psi_{1/2}$ is given by

$$\psi_{1/2} = 0.8 F_{RS}(\xi)\psi_1, \tag{5}$$

where, for axial channeling,

$$\psi_1 = 0.307\left(\frac{Z_1 Z_2}{Ed}\right)^{1/2} \text{(degrees)}, \tag{6}$$

and $F_{RS}(\xi)$ is the square root of continuum Moliere potential, evaluated at ξ. E is the ion energy expressed in MeV, d is the average interatomic distance (in Å) along the channeling axis. When there are different types of atoms in a row along the channeling axis, Z_2 is replaced by the average Z_2. $\xi = 1.2u_1/a$, where a is the Thomas-Fermi screening radius given by

$$a = \frac{0.4685}{(Z_1^{1/2} + Z_2^{1/2})^{2/3}}, \tag{7}$$

and u_1 is the one-dimensional root-mean-square vibrational amplitude.

The ratio of the backscattering yield for the aligned condition (RBS with channeling) to that for the random incidence (RBS without channeling) of the ion beam is denoted by $\chi_{\min}$ and called the *minimum yield.* It is a measure of the crystalline quality of the sample. $\chi_{\min}$ is given by

$$\chi_{\min} = N_a d\pi(2u_1^2 + a^2), \tag{8}$$

where N_a is the number of atoms/Å^3. For a good crystal at room temperature $\chi_{\min}$ is typically a few per cent.

Typical RBS spectra for an ion beam incident along a crystallographic axis are shown in Figure 3. The tiny peak originating from scattering by surface atoms, is called *surface peak.* This can be understood from Figure 2. On an atomic string, ions cannot reach the region within the *shadow cone* behind the surface atom. This means that only the surface atoms would produce backscattered ions. Other atoms behind the surface atom would not see the incident ions and hence would not produce backscattered ions. However, atoms undergo thermal vibration. Even at absolute zero temperature they have zero-point motion. Thus the vibrating atoms in the atomic row have a finite probability of coming out of the shadow-cone region and produce backscattering of ions. In essence, a surface atom scatters with full probability, and the atoms behind scatter with reduced probabilities. Effectively a few atoms per atomic row generate the backscattering signal producing the *surface peak.* From larger depths the backscattering yield is reduced. The yield from larger depths is mainly from scattering of dechanneled ions. $\chi_{\min}$ is the average yield-ratio taken over a narrow window below the surface peak (Figure 3).

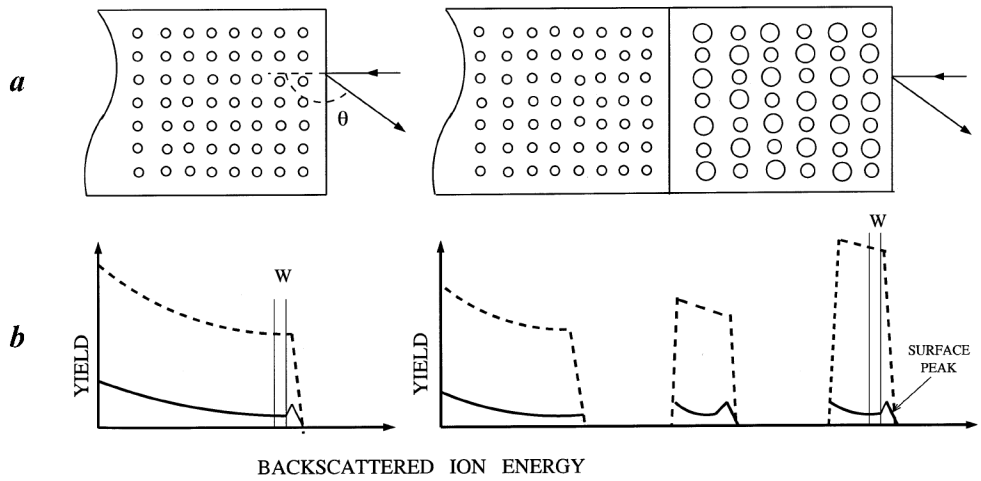

Figure 3. Schematic backscattering spectra of (*a*) a monoelemental crystal substrate and (*b*) a thin film (compound) on this substrate under channeling condition (solid lines) and without channeling (dashed lines). χ_{min} is the yield ratio taken within a narrow window (W) below the surface peak. (See text for details.)

2.3 *Some applications of the combined RBS/channeling technique*

On a clean crystal surface, atoms usually occupy positions displaced from their ideal site giving rise to what is called *surface reconstruction* and *surface relaxation*. Elaborating on these core topics in surface physics is beyond the scope of this article. However, it is easy to appreciate how these aspects can be studied using RBS and channeling. Imagine that the top atom on each atomic string is displaced laterally. Then the second atom is also exposed to the incident ions and hence both the first and the second atom scatter with full probability and effectively the yield in the *surface peak* would be higher. This yield can be compared with that obtained from Monte-Carlo simulations for various surface structural models to determine the surface structure. This is how structure of bare surfaces and of surfaces with adsorbed atoms, surface structural phase transitions and growth modes in epitaxial growth are studied[2,3].

Various aspects of thin epitaxial crystalline layers grown on various crystalline substrates can be analysed by the application of combined RBS and channeling. Determination of mismatch in crystallographic orientation, analysis of strain in the epitaxial layers and determination of defects (type and density) are possible. Some examples of these are discussed in §5 and 6.

From Figure 2, it is clear that an impurity atom at a substitutional site would be embedded in the atomic string of the host crystal and thus produce low backscattering yield under channeling condition. However, an interstitial impurity atom would reside between adjacent atomic strings. So the channeled ions would be strongly backscattered by the interstitial impurity atoms. Thus the RBS/channeling technique can provide information about the location of impurity atoms in the crystal lattice. This is discussed in §7.

Lattice damage, present in the surface region, also produces higher *surface peak* yield. Thus an analysis of the surface peak can provide information about lattice damage produced in the surface region in ion–solid interaction. This aspect has been utilized in the study of interference effects in the interaction of cluster ions with solids and presented in §8.

3. Surface passivation and the diffusion barrier across an interface

Surfaces of materials are usually reactive and react with the species present in its environment. This is why surface oxidation is a common phenomenon. A silicon surface, when left in air, attains ~ 15 Å of SiO_x (native oxide). If a thin film of any material is grown on such an oxidized substrate, the oxide layer acts as a diffusion barrier for atomic diffusion across the film/substrate interface. This barrier at the interface for interdiffusion is significantly lowered when the thin film is grown on an atomically clean surface[7]. However, experiments involving clean surfaces require an ultrahigh vacuum (pressure: ~ 10^{-10} mbar) environment involving expensive equipments. It has been shown that interesting work in the area of surface and interface studies can be performed even under high vacuum (pressure: ~ 10^{-6} mbar) conditions, which are easy to obtain, if a nonreactive (passive) surface is used for thin film growth. This was first demonstrated for the case where silicon surfaces were chemically passivated by adsorption of bromine and thin films were grown on the passivated surface[6,8]. Si(111) surface can be passivated by Br-chemisorption. However, Si(100) surface cannot be

effectively passivated by Br (refs 8, 9). This is illustrated in Figure 4 in terms of dangling bonds on the respective surfaces.

RBS measurements show that the diffusion barrier at the interface between a Cu film on an atomically clean Si surface (Cu/Si) and that at the interface between Cu and Br-passivated Si(111) surface (Cu/Br–Si(111)) are comparable – both significantly lower compared to the barrier in the presence of an oxide layer at the interface[6,8]. In other words, the behaviour of the Br–Si(111) surface is very similar to that of an atomically clean Si surface, which can only be prepared under ultrahigh vacuum conditions. This finding has enabled a large number of subsequent interesting studies involving Br-passivated Si(111) surfaces. For the Cu/Br–Si(111) system the onset of diffusion across the interface takes place at an annealing temperature of 220°C as observed in RBS results (Figure 5) (ref. 6). At 300°C, a significant diffusion of Cu into Si was detected and the diffusion coefficient (3×10^{-14} cm^2/s) was determined from the RBS spectrum[6].

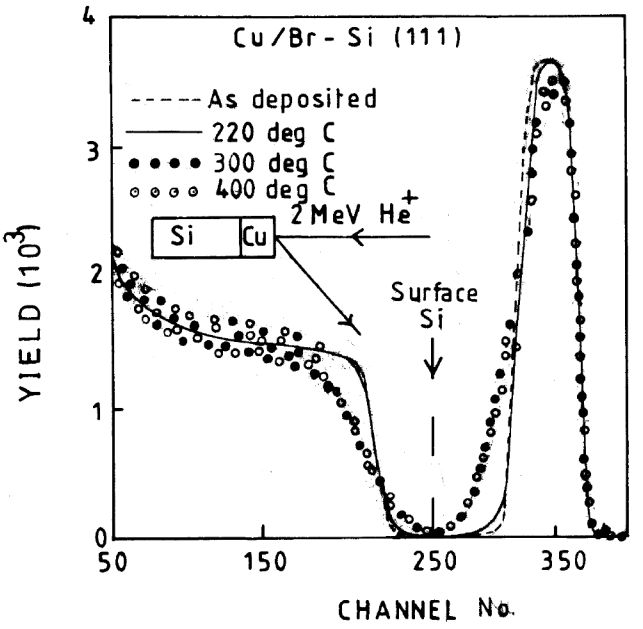

Figure 5. RBS spectra of Cu thin films on Br-passivated Si(111) surfaces showing interdiffusion at different annealing temperatures. Yields above channel number (energy) 270 are from scattering by Cu (above channel number 310 for the as-deposited layer). The tailing of the Cu signal towards lower channel no. for annealed samples indicates diffusion of Cu into Si. (from ref. 6).

4. Self-organized structures on semiconductor surfaces

Growth of self-organized structures on Br–Si(111) surfaces has been studied by IBA in conjunction with many other techniques. Here we discuss heteroepitaxial structures. There are three possible growth modes depending on the free energy of the substrate material (σ_s), that of the deposited material (σ_o) and the lattice mismatch between them. If $\sigma_s > \sigma_o$, usually the overlayer grows in layer-by-layer or layer-plus-island mode. Lattice mismatch makes the overlayer strained. The strain relaxation may take place via introduction of dislocations and/or shape transition[10]. The first experimental results on shape transition were provided by us with the self-assembled epitaxial growth of gold silicide on Br–S(111) surfaces[11]. About 1000 Å Au was deposited under high vacuum conditions on a Br–Si(111) substrate. The sample was annealed at 360 ± 10°C, i.e., close to the Au–Si eutectic temperature (363°C). This produced epitaxial Au_4Si islands in the shapes of equilateral triangle and trapezoid. Small islands grew following the tree-fold symmetry of the Si(111) surface up to a critical size. Larger islands underwent a shape transition: equilateral triangle to trapezoid[11]. The RBS spectra from an as-deposited Au layer on Br–Si(111) surface and from an annealed sample are shown in Figure 6. The tailing of the Au signal into lower energy region has two possible interpretations – namely, diffusion of Au into Si, like that in Figure 5, and the second interpretation is that the layer has nonuniform thickness. In the case of annealed Au/Br–Si(111) system, it is the second reason that has caused the tailing[12]. This is evident in the optical micrograph shown in Figure 7. Au_4Si islands and gold in stringy pattern are seen in the

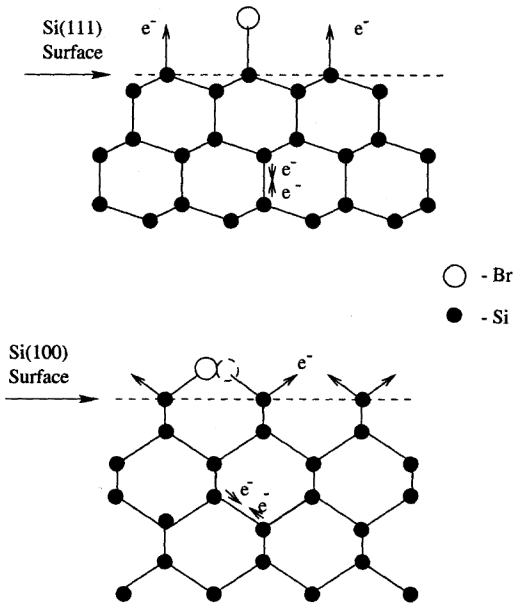

Figure 4. Ideal Si(111) and Si(100) surfaces are shown. While in bulk Si, two neighbouring Si atoms contribute one electron (e^-) each to form a covalent bond, surface Si atoms have unsaturated 'dangling' bonds with one electron. Because of these dangling bonds the surface is reactive. Dangling bonds can be passivated by bonding with halogen (group VII) atoms like Br. While this is simple on Si(111) surface (*a*), it is otherwise on Si(100) surface (*b*) as Br on two neighbouring dangling bonds would require them to be too close to be allowed. Thus, while passivation of Si(111) surface by Br is obtained, effective passivation of Si(100) surface is not observed.

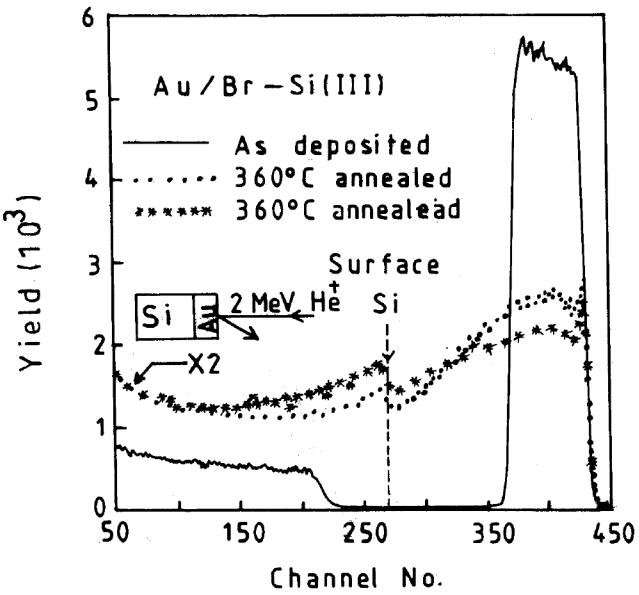

Figure 6. RBS spectra from an as-deposited Au layer on a Br–Si(111) substrate and from two different spots on an annealed sample. For the annealed sample the tailing of the signal from Au towards lower channel numbers (< 365) is due to formation of thick structures of gold silicide islands and Au fractals (see text). (from ref. 12).

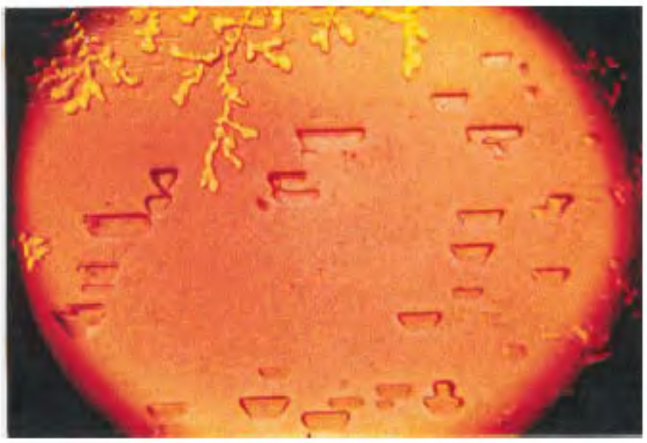

Figure 7. An optical micrograph of an annealed (360°C) Au/Br–Si(111) sample showing triangular and trapezoidal gold silicide islands. The background layer, with the same colour as that of the islands, is also gold silicide. The stringy golden pattern is Au. Field of view: 400 μm. (from ref. 11).

micrograph. Au_4Si islands are epitaxial as revealed in RBS/channeling experiments (Figure 8)[13]. The silicide islands are much thicker in comparison to the initial Au film thickness. This is evident from the width of the RBS signal from Au (Figure 8) as well as secondary ion mass spectrometry (SIMS) measurements on individual islands[14]. Au_4Si islands are strained because of lattice parameter mismatch between Au_4Si and Si. The shape transition (Figure 9) has taken place as a mechanism for strain relaxation[10,11]. Shape transition has later been

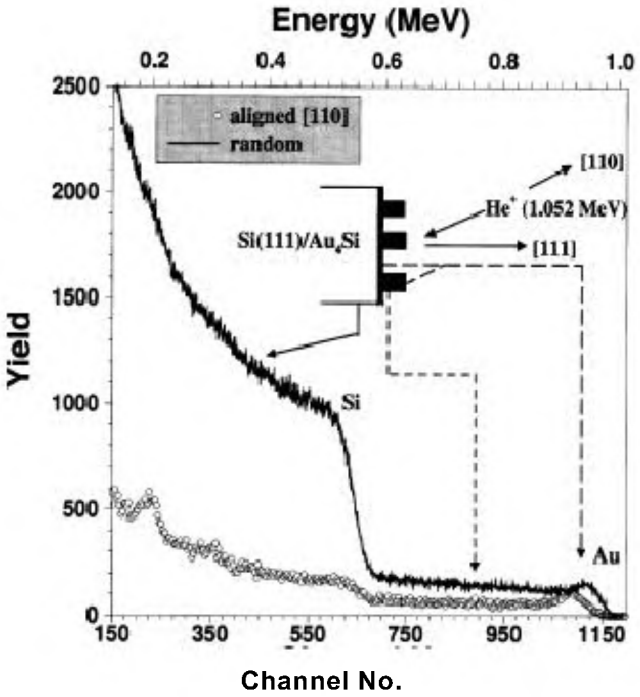

Figure 8. RBS/channeling spectra from an annealed (360°C) Au/Br–Si(111) sample. Unreacted Au was removed by etching in aqua-regia. So the spectra represent the gold silicide/Si system. Reduced yield under axial channeling condition confirms the crystallinity of silicide and its epitaxy on Si. (from ref. 13).

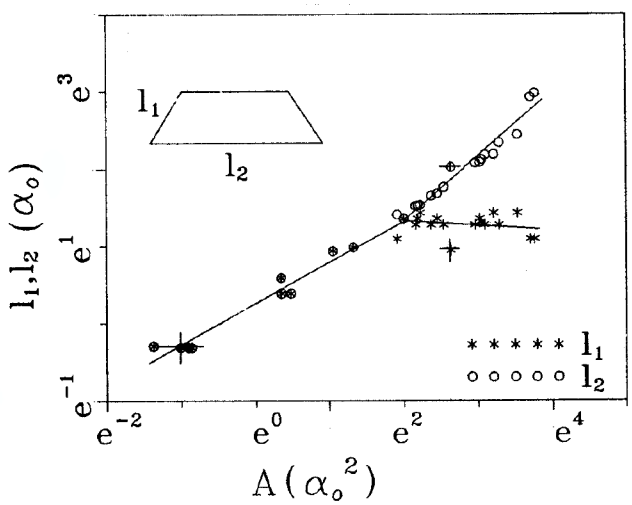

Figure 9. From micrographs like those in Figure 7, silicide island dimensions (l_1, l_2) are plotted against island area in units of critical dimension α_0. Equilateral triangular islands ($l_1 = l_2$) grows up to a critical size beyond which shape transition to trapezoidal islands ($l_2 > l_1$) takes place. This is an effect of strain relaxation in the gold-silicide/silicon heteroepitaxial system. (from ref. 11).

observed in other systems, prepared by other methods[15]. Self-organized growth involving shape transition can give rise to formation of *quantum wires*. The stringy patterns of Au in Figure 7 are induced by the epitaxial growth of the Au_4Si islands and they are actually fractal structures with an average Hausdorff dimension of 1.69 (ref. 16).

5. Growth of epitaxial layers on vicinal surfaces and IBA

When a crystal is cut in such a way that the crystal surface has a small (usually a few degrees) angle with respect to a lattice plane, the surface is called a vicinal surface. Vicinal surfaces are useful in growing quantum structures on them. This makes the study of growth of epitaxial layers on vicinal surfaces interesting. It is known that a vicinal surface, due to the miscut of substrate from a low index plane, induces a tilt of the epilayer that is grown on it. Tilted misfit dislocations are also known to result in a tilt when there is a net excess of vertical edge component of the Burgers vector at the interface. Without this tilt the vertical edge components, unnecessary for the relaxation of lattice mismatch, induce a long range stress field. Thus the study of overlayer tilt and stress (or strain) is important.

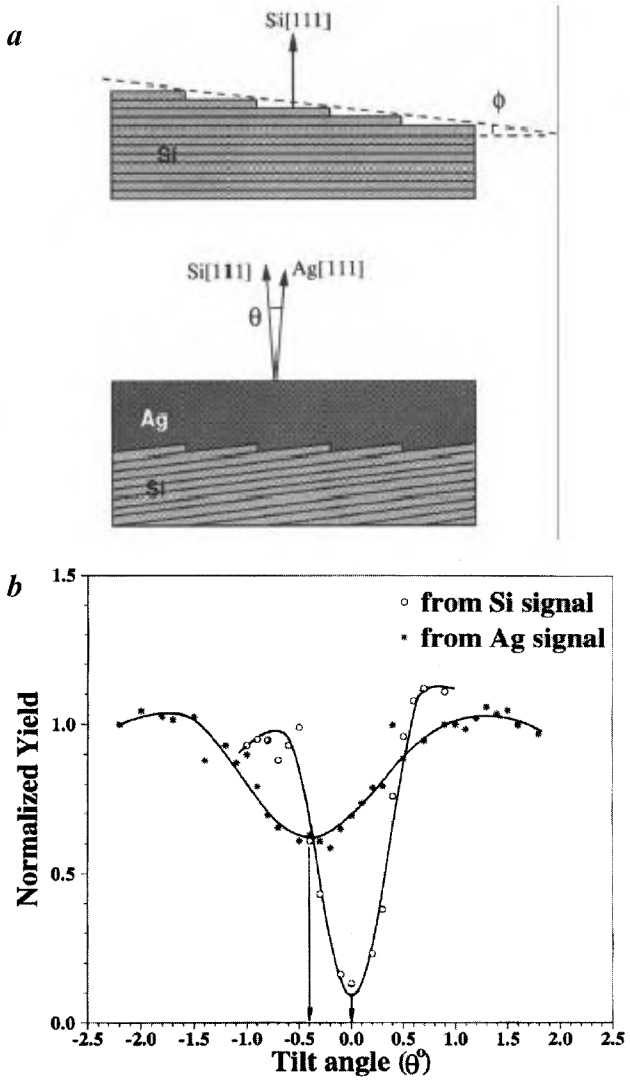

Figure 10. *a*, Vicinal Si(111) surface. The vicinal angle (ϕ) between Si surface and Si(111) planes is 4°. Such surfaces are stepped. Growth of an epitaxial Ag(111) layer on this vicinal Si(111) surface produces a tilt (θ) between Si[111] and Ag[111] crystallographic directions. *b*, The value of this tilt is obtained from RBS/channeling spectra as the difference in angular positions in channeling dips. Here the measured tilt is $\theta = 0.4°$. Here tilt angle (θ) indicates the direction of the incident ion beam w.r.t. the Si[111] direction. The yield values were obtained over an energy window, as shown in Figure 3, from a large no. of RBS spectra. (from ref. 17). [Reprinted from *Appl. Surface Sci.*, Volume number 137, pp. 11–19, Copyright (1999), with permission from Elsevier Science.]

We have studied the growth of Ag epilayers on vicinal Si(111) surfaces (4° miscut) by RBS/channeling and other techniques. The measurements of the tilt between Ag[111] and Si[111] directions are shown in Figure 10. The tilt angle is directly obtained from the separation between the angular positions of the channeling dips (Figure 10 *b*). The detailed analysis of strain, mosaic spread and thermal annealing behaviour are described in ref. 17.

The Ag layer is grainy. This leads to interesting changes in morphology upon thermal annealing. At 600°C, where Ag desorption takes place, faceted holes are formed. At 700°C when Ag vapour pressure is much higher, fractal holes are formed[18]. It was shown that the crystalline quality of the Ag layer can be improved by irradiating the layers by MeV ions[19].

6. Synthesis and analysis of heteroepitaxial layers

Ion beam synthesis of buried layers in single crystalline silicon started about twenty years ago[20]. This technique, named SIMOX (separation by implantation of oxygen) meets industrial standards and allows the fabrication of high performance devices[21]. The first successful synthesis of buried epitaxial silicides was achieved by White *et al.*[22]. The process of ion beam synthesis of an epitaxial layer is schematically shown in Figure 11. $CoSi_2$/Si interface provides a Schottky barrier, an essential component in fast modern electronic devices. Buried epitaxial cobalt silicide ($CoSi_2$) layers in single crystalline Si have been prepared by ion beam synthesis. Various aspects of analysis of this Si(880 Å)/$CoSi_2$(680 Å)/Si system have been published by our group[23–27]. An interface may have structural twinning, which alters Schottky barrier height. Whether the $CoSi_2$/Si interfaces have twinning has been determined

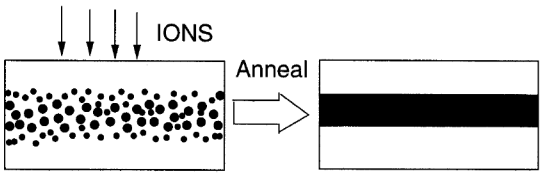

Figure 11. High dose ion implantation at an elevated substrate temperature followed by a post-implantation annealing can produce a buried epitaxial layer of the reacted material with sharp interfaces. Co^+ implantation into Si can produce a buried $CoSi_2$ epitaxial layer in Si (Si/$CoSi_2$/Si). Schottky barriers are formed at the Si/$CoSi_2$ interfaces.

by IBA[23]. Both $CoSi_2$ and Si have cubic unit cells with a lattice parameter mismatch of 1.2%. This introduces a strain in the $CoSi_2$ layer. Both the parallel and the perpendicular components of the strain have been determined[24]. For a layer thickness exceeding a critical value, defects are introduced in the system as a mechanism for strain relaxation. Type of defects has been identified and the density of defects has been determined by RBS/channeling experiments[25,26]. Some of these aspects have also been reviewed[27].

GeSi alloy layers epitaxially grown on Si or Ge, have drawn considerable attention due to their potential use for band gap engineering and their compatibility with modern VLSI and ULSI technology. $Si/Si_{1-x}Ge_x$ or $Ge/Ge_{1-x}Si_x$ heterojunction bipolar transistors are candidates for extending high frequency limits of Si and Ge based bipolar transistors. Ion beam synthesis has been used to fabricate buried $Ge_{1-x}Si_x$ layers in Ge ($Ge/Ge_{1-x}Si_x/Ge$) by implanting 1 MeV Si^+ ions into Ge. Detailed analyses of this system have been presented by Kuri *et al.*[28].

Crystalline quality of the epilayer and the Al concentration have been determined in liquid phase epitaxy (LPE)-grown $Al_xGa_{1-x}As/GaAs(111)$ systems[29]. As GaAs and AlAs are lattice matched $Al_xGa_{1-x}As$ layers grow on GaAs as strain-free layers. The larger lattice constant of InAs compared to GaAs makes the $In_xGa_{1-x}As$ layers on GaAs strained. Lattice strain in organometallic vapour phase epitaxy (OMVPE)-grown strained $In_xGa_{1-x}As/GaAs$ heteroepitaxial systems has been measured by IBA[30].

7. Ion beam induced surface and near-surface modifications

Various properties of materials are modified by incorporating ions into a shallow region (≤ a few hundred nm and sometimes deeper) below the surface of materials by ion implantation.

Semiconductors with *n*- and *p*-type carriers are obtained by doping with impurities, conveniently done by ion implantation. Whether the carrier is active depends on whether the impurity atoms have occupied substitutional site. Incorporation of impurities by IBM and the determination of their position(s) in the crystalline lattice by IBA are standard practices. Both these aspects with As and Sb impurity incorporation into Si with MeV As^+ and Sb^{2+} ions and analysis with MeV He^+ ions are discussed in references 31 and 32.

Buried high resistance region provides the basis for isolation and low optical loss in semiconductor optoelectronic devices. MeV ion implantation has the advantage of producing a buried semi-insulating layer which is attractive for vertical isolation of surface devices from the conducting substrate. The outstanding physical properties, such as advantageous band gap energy and the high electron mobility make InP a basic material for optoelectronic and microwave applications. Recently transition metal implants were used to compensate donor implant tails and to obtain high resistance layers in *n*-type InP. We have studied ~ 1 MeV Ni^+ implantation into Sn-doped InP(100) crystals for damage creation, annealing behaviour and Ni redistribution[33].

IBM can drastically modify the vaporization behaviour of materials by changing the nature of the near-surface region. We have studied this aspect for Au implantation in GaAs crystals[34]. Ion implantation also modifies surface roughness. Roughness enhancements have been observed for Au^{++} implantation into $LiNbO_3$ and Co^+ implantation into Si. Ion dose dependence of roughness has also been studied[35].

Nanoclusters can be produced in a variety of insulators by ion implantation. The quantum dot composites fabricated by implantation of metal ions into a dielectric can be used for fabricating nonlinear waveguide and other photonic devices[36,37]. We have studied the early stage of clustering process of implanted metal atoms in dielectrics, involving implantation of MeV Au^{++} ions into $LiNbO_3$ followed by RBS and channeling studies using an MeV B^{++} beam[38].

8. Cluster–ion interaction with solids

The virtue of cluster ion implantation has been recognized only in recent years. An interesting aspect of cluster ion beam interaction with solids lies in the coherent dynamic response of the electrons in the solid giving rise to a modified electronic stopping power through an interference effect. This effect is expected to be prominent only in the near-surface region[39,40].

The case of H_3^+-molecular ion beam interacting with amorphous carbon targets has been explicitly worked out[40]. After the H_3^+-molecular (cluster) ion enters into the target, the constituent protons get separated due to Coulomb repulsion. Nevertheless, over a small depth under the surface of the target they are close enough to display correlated behaviour. Thus the stopping power of the H_3^+ cluser ($S_{H_3^+}$) is different from the stopping power of its constituents taken individually ($3S_p$)[40].

$$S_{H_3^+}(r) = \left[\sum_{i=1}^{3} Z_i^{*2} + \sum_{i \neq j}^{3} Z_i^* Z_j^* I(r)\right] S_p, \tag{9}$$

where Z_i^* is the effective charge of each proton in the cluster, S_p is the proton stopping power and the interference function $I(r)$ accounts for the collective effects that appear in the stopping power of correlated particles, r being the variable internuclear separation between the constituents of the cluster ion. As the cluster ion pene-

trates into the target, r increases and eventually r becomes so large that the constituents are like independent particles showing no interference ($I(r) = 0$). Thus the second term in eq. (9) has no contribution at such higher penetration depths. For carbon foil targets an enhancement factor of ~ 1.5 in the H_3^+ stopping power ($S_{H_3^+}/3S_p \sim 1.5$) was theoretically obtained in the near-surface region (< 10 nm from the surface) for the ion energy range of 60–120 keV/amu. The calculated values agree well with those from experiments.

Since the interference effect is dominant only within a very thin surface layer ($\lesssim 10$ nm) it would be ideal to prepare self-supporting thin film ($\lesssim 10$ nm) samples and study the energy loss of ions in transmission through them. However, it is difficult to prepare self-supporting thin films of this dimension. Secondly, measuring very small energy loss in transmission through this thin layer and the difference in energy losses requires sophistication in experimental techniques. We adopted an alternative method to study the interference effect through the study of an effect that the electronic stopping power or energy loss produces in the target. Energy deposition into an insulating or a semi-insulating solid by the ions through electronic excitation can cause lattice damage via electron–phonon coupling. We have determined the surface damage in semi-insulating GaAs(001) crystals in C^+ and C_2^+ irradiation by the RBS-channeling technique. We used 1 MeV C^+ and 2 MeV C_2^+ ions (same energy/mass: 83.3 keV/amu) with the same atomic dose (C^+: 5×10^{14}, C_2^+: 2.5×10^{14} ions/cm^2) (ref. 41). The results are shown in Figure 12. Higher surface peak yield indicates higher damage. The damage is confined mainly within a depth of ~ 10 nm from the surface. The higher damage caused by C_2^+ implantation is an indication of $S_{C_2^+} > 2S_{C^+}$, thus showing a coherent dynamic response of the target in electronic stopping power. At this ion energy the electronic stopping is the dominant energy loss mechanism (electronic: 1090 eV/nm, nuclear: 13 eV/nm).

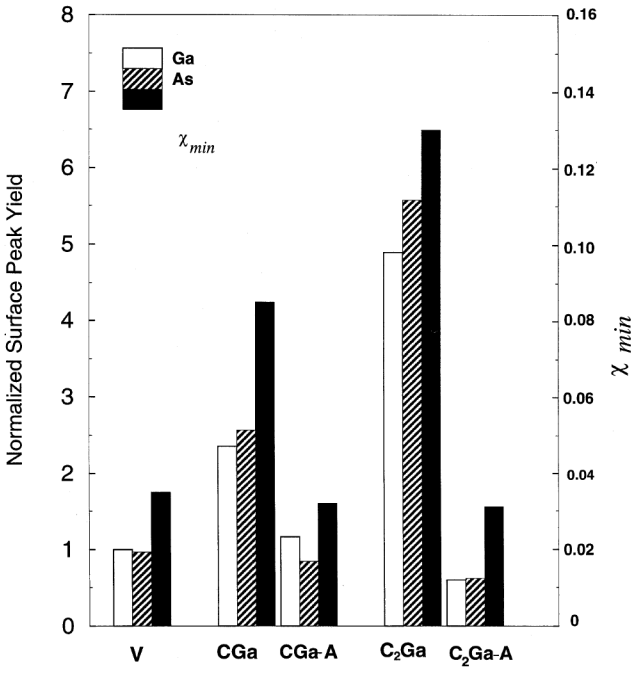

Figure 12. Ga and As surface peak yields and minimum yield (χ_{min}) obtained from RBS/channeling measurements on semi-insulating GaAs(001) crystals irradiated with C^+ and C_2^+ ions. Higher surface peak yield indicates higher surface damage. Lower minimum yield indicates better crystallinity. In symbols like C_2Ga-A 'Ga' represents Ga co-implantation at identical conditions. 'A' represents annealed samples. Higher damage observed for C_2^+ in comparison to C^+ irradiation indicates a coherent dynamic effect in cluster irradiation. V indicates virgin (unirradiated) sample. Annealing removes damage significantly and improves crystalline quality. (from ref. 41). [Reprinted from *Nucl. Instrum. Methods Phys. Res. B*, Volume number 156, pp. 125–129, Copyright (1999), with permission from Elsevier Science.]

9. Studies of microstructures with an ion microprobe

An ion microbeam facility has been developed at one of the beam lines of our Pelletron accelerator[42,43]. We have obtained a beam size of ~ 3 μm diameter (full width at half maximum). Three dimensional RBS mapping of epitaxial microstructures of gold silicide islands on Si(110) surfaces was demonstrated[43]. Detailed RBS studies with an ion microbeam on self-assembled gold silicide wire structures on Si(110) surfaces helped understanding the growth mode, silicide composition and epitaxial structural relationship between the silicide wires and the underlying silicon[44]. We have recently studied MeV ion beam induced mass transport on epitaxial Ag(111) layers on Si(111) surfaces by micro-RBS measurements[45,46].

10. Conclusions and outlook

By ion beam analysis we have demonstrated the equivalence between atomically clean Si(111) surface prepared under UHV conditions and chemically bromine-passivated Si(111) surface as far as diffusion across the interface is concerned, when a thin film is deposited on them. Using the Br–Si(111) substrates for thin film growth, we gave the first experimental results on the phenomenon of shape transition in heteroepitaxial growth. Our ion beam modification studies have involved fabrication of buried electrically active layers, insulating layers, epitaxial layers with Schottky barrier interfaces, metal nanoclusters in dielectrics, improvement of crystalline quality of epilayers and surface modifications such as surface roughness and vaporization behaviour. Ion beam analysis involved studies of diffusion across interfaces, crystalline quality, lattice location of impurity atoms in crystals, besides interface twinning, strain and defects in epitaxial layers. The study of interaction of cluster-ions with solids showed

an interference effect in electronic stopping power due to coherent dynamic response of the electrons in the solid because of the vicinage of the constituents of the cluster ion.

For the study of atomically clean surfaces, interfaces and epilayers, we have assembled a UHV equipment at one of the beam lines. The chamber vacuum is $\sim 10^{-10}$ mbar. It is fitted with an Ar^+ sputter gun, a low energy electron diffraction (LEED)/Auger electron spectroscopy (AES) system, effusion cells and a precision goniometer and connected to ion beam from the Pelletron for RBS/channeling measurements[46]. This *in situ* ion scattering facility will enable us to tackle more challenging problems in surface physics.

1. See for example, *Ion Beam Modification of Materials* (eds S. Kalbitzer, O. Mayer and G. K. Wolf), North-Holland, Amsterdam, 1993, Part I & II; *Nucl. Instrum. Methods*, 1993, B80/81.
2. Feldman, L. C. and Mayer, J. W., *Fundamentals of Surface and Thin Film Analysis*, North-Holland, New York, 1986, pp. 113–123.
3. van der Veen, J. F., *Surface Sci. Rep.*, 1985, **5**,199–287.
4. Dev, B. N., *Curr. Sci.*, 2000, **78**, 1511–1514.
5. Sekar, K., Kuri, G., Satyam, P. V., Sundaravel, B., Mahapatra, D. P. and Dev, B. N., *Indian J. Phys.*, 1994, **A68**, 1–22.
6. Sekar, K., Satyam, P. V., Kuri, G., Mahapatra, D. P. and Dev, B. N., *Nucl. Instrum. Methods*, 1993, **B73**, 63–70.
7. Nakahara, T., Okhura, S., Shoji, F., Hanawa, T. and Oura, K., *Nucl. Instrum. Methods*, 1990, **B45**, 467–470.
8. Sekar, K., Satyam, P. V., Kuri, G., Mahapatra, D. P. and Dev, B. N., *Nucl. Instrum. Methods*, 1992, **B71**, 308–313.
9. Sekar, K., Kuri, G., Mahapatra, D. P., Dev, B. N., Ramana, J. V., Kumar, S. and Raju, V. S., *Surface Sci.*, 1994, **302**, 25–36.
10. Tersoff, J. and Tromp, R. M., *Phys. Rev. Lett.*, 1993, **70**, 2782–2785.
11. Sekar, K., Kuri, G., Satyam, P. V., Sundaravel, B., Mahapatra, D. P. and Dev, B. N., *Phys. Rev.*, 1995, **B51**, 14330–14336.
12. Sekar, K., Kuri, G., Satyam, P. V., Sundaravel, B., Mahapatra, D. P. and Dev, B. N., *Surface Sci.*, 1995, **339**, 96–104.
13. Sundaravel, B., Sekar, K., Satyam, P. V., Kuri, G., Rout, B., Ghose, S. K., Mahapatra, D. P. and Dev, B. N., *Indian J. Phys.*, 1996, **A70**, 681–685.
14. Sundaravel, B., Sekar, K., Kuri, G., Satyam, P. V., Dev, B. N., Bera, Santanu, Narasimhan, S. V. Chakraborty, P. and Caccavale, F., *Appl. Surface Sci.*, 1999, **137**, 103–112.
15. Brongersma, S. H., Castell, M. R., Perovic, D. D. and Zinke-Allmang, M., *Phys. Rev. Lett.*, 1998, **80**, 3795–3798.
16. Sekar, K., Kuri, G., Satyam, P. V., Sundaravel, B., Mahapatra, D. P. and Dev, B. N., *Solid State Commun.*, 1995, **96**, 871–875.
17. Sundaravel, B., Das, Amal, K., Ghose, S. K., Sekar, K. and Dev, B. N., *Appl. Surface Sci.*, 1999, **137**, 11–19.
18. Sundaravel, B., Das, Amal, K., Ghose, S. K. and Dev, B. N., *Solid State Physics*, 1997, **C40**, 400.
19. Sundaravel, B., Das, Amal, K., Rout, B. and Dev, B. N., *Nucl. Instrum. Methods*, 1999, **B156**, 130–134.
20. Izumi, K., Doken, M. and Arigoshi, H., *Electron. Lett.*, 1978, **14**, 593–597.
21. Colinge, J.-P., *Silicon-on-Insulator Technology: Materials to VLSI*, Kluwer, Boston, 1991.
22. White, A. E., Short, K. T., Dynes, R. C., Garno, J. P. and Gibson, J. M., *Appl. Phys. Lett.*, 1987, **50**, 95–97.
23. Satyam, P. V., Sekar, K., Kuri, G., Sundaravel, B., Mahapatra, D. P. and Dev, B. N., *Indian J. Phys.*, 1996, **A70**, 777–782.
24. Satyam, P. V., Sundaravel, B., Ghose, S. K., Rout, B., Sekar, K., Mahapatra, D. P. and Dev, B. N., *Indian J. Phys.*, 1996, **A70**, 783–790.
25. Satyam, P. V., Sekar, K., Kuri, G., Sundaravel, B., Mahapatra, D. P. and Dev, B. N., *Philos. Mag. Lett.*, 1996, **73**, 309–317.
26. Satyam, P. V., Sekar, K., Kuri, G., Sundaravel, B., Mahapatra, D. P. and Dev, B. N., *Appl. Surface Sci.*, 1998, **125**, 173–177.
27. Dev, B. N., *Nucl. Instrum. Methods*, 1999, **B156**, 258–264.
28. Kuri, G., Mahapatra, D. P. and Dev, B. N., *Radiation Effects and Defects in Solids*, 1999, **147**, 133–149.
29. Kuri, G., Satyam, P. V., Sundaravel, B., Sekar, K., Mahapatra, D. P. and Dev, B. N., *Nucl. Instrum Methods*, 1998, **B140**, 229–234.
30. Siddiqui, A. M., Pathak, A. P., Sundaravel, B., Das, Amal, K., Sekar, K., Dev, B. N. and Arora, B. M., *Nucl. Instrum. Methods*, 1998, **B142**, 387–392.
31. Kuri, G., Sundaravel, B., Rout, B., Mahapatra, D. P. and Dev, B. N., *Nucl. Instrum. Methods*, 1996, **B111**, 234–243.
32. Dey, S., Kuri, G., Rout, B. and Varma, S., *Nucl. Instrum. Methods*, 1998, **B142**, 35–42.
33. Chini, T. K., Bhattacharyya, S. R., Basu, D., Rout, B., Ghose, S. K., Sundaravel, B., Dev, B. N., Okuyama, F. and Kaneko, M., *J. Mater. Sci. Lett.*, 1998, **17**, 1117–1119.
34. Kuri, G., Rout, B., Sundarvel, B., Mahapatra, D. P. and Dev, B. N., *Nucl. Instrum. Methods*, 1996, **B119**, 403–410.
35. Satyam, P. V., Bhar, D., Ghose, S. K., Kuri, G., Sundaravel, B., Rout, B. and Dev, B. N., *Curr. Sci.*, 1995, **69**, 526–529.
36. Haglund Jr., R. F., Yang Li, Magruder-III, R. H., White, C. W., Zuhr, R. A., Yang, L., Dorsinville, R. and Alfano, R. R., *Nucl. Instrum. Methods*, 1994, **B91**, 493–504.
37. Chakraborty, P., *J. Mater. Sci.*, 1998, **33**, 2235–2249.
38. Dev, B. N., Kuri, G., Satyam, P. V., Sundaravel, B., Gog, Th. and Materlik, G., *Appl. Surface Sci.*, 1998, **125**, 163–172.
39. Brandt, W., Ratkowsky, A. and Ritchie, R. H., *Phys. Rev. Lett.*, 1974, **33**, 1325–1328.
40. Denton, C., Perez-Perez, F. J., Abril, I., Garcia-Molina, R. and Arista, N. R., *Europhys. Lett.*, 1996, **35**, 499–504.
41. Ghose, S. K., Kuri, G., Das, Amal, K., Rout, B., Mahapatra, D. P. and Dev, B. N., *Nucl. Instrum. Methods*, 1999, **B156**, 125–129.
42. Rout, B., Ghose, S. K., Sundaravel, B., Kuri, G., Mahapatra, D. P., Dev, B. N., Sen, P., Bakhru, H. and Haberl, A. W., *Radiat. Phys. Chem.*, 1998, **51**, 677.
43. Rout, B., Ghose, S. K., Dey, S., Mahapatra, D. P., Dev, B. N., Bakhru, H. and Haberl, A. W., *Indian J. Pure Appl. Phys.* 2001, **39**, 62–64.
44. Rout, B., Sundaravel, B., Das, Amal, K., Ghose, S. K., Sekar, K., Mahapatra, D. P. and Dev, B. N., *J. Vac. Sci. Technol.*, 2000, **B18**, 1847–1852.
45. Rout, B., Kamila, J., Ghose, S. K., Mahapatra, D. P. and Dev, B. N., 7th International Conference on Nuclear Microprobe Technology & Applications, Bordeaux, France, September 10–15, 2000; *Nucl. Instrum. Methods*, 2001, B (in press).
46. Rout, B., Ph D thesis, Utkal University, 2001.

ACKNOWLEDGEMENTS. I thank Drs K. Sekar, P.V. Satyam, G. Kuri and B. Sundaravel, who contributed to this research programme during their thesis work, Dr T. Chini, Research scholars B. Rout, S.K. Ghose, Amal K. Das, J. Kamila, D.K. Goswami, and Prof. D.P. Mahapatra. I also acknowledge the help given by the technical staff of our Ion Beam Laboratory.